Air Flow and Particle Trajectories around Aircraft Fuselages. II: Measurements

W. D. KING, D. E. TURVEY, D. WILLIAMS AND D. J. LLEWELLYN

Cloud Physics Laboratory, Division of Atmospheric Research, CSIRO, Sydney, Australia

(Manuscript received 26 August 1983, in final form 18 December 1983)

ABSTRACT

Measurements have been made of airflow velocities and cloud liquid water contents from selected positions around the fuselage of an F-27 aircraft. The airflow measurements away from the propeller inflow region are in reasonable agreement with those calculated in Part I. The liquid water measurements were made using two CSIRO hot-wire probes, one of which could be positioned at distances of 15–60 cm from the fuselage. Results of these comparisons showed that the enhancement factors calculated in Part I appear quite reasonable and that corrections can consequently be made to allow for sampling errors caused by fuselage-related flow distortions. The comparisons also show that there are additional sampling errors as large as 10% which depend on position of the probe relative to the wings and propellers. For the F-27 these additional effects decrease substantially with increasing aircraft speed.

1. Introduction

In King (1983, hereafter Part I) we showed that the airflow around aircraft fuselage slopes could be computed fairly simply using a distributed sink–source technique. As a consequence of these calculations it was shown that away from the immediate nose area the flow velocities depend primarily on the distance from the nose, scaled in terms of the fuselage radius in the plane of interest. In this paper, as in I, any "scaled" or "normalized" dimension is that dimension divided by the fuselage radius. Similarly the particle trajectories around the fuselage (and related concentration enhancement factors) depend on the normalized distance from the fuselage and nondimensional parameter defined by $S = 2a^2V\rho_w/9\eta b$, where a is the droplet radius, V the free-stream velocity, ρ_w the density of water, η the viscosity of air and b the fuselage radius.

In this paper, we compare the theory of Part I with some measurements of airflow velocities and liquid water content (LWC) at various distances from the fuselage of a Fokker F-27. The results of these comparisons at various fuselage locations are used to assess the relative importance of sampling errors due to flows associated with the fuselage, the wings and propellers.

2. Measurement techniques

All the measurements were obtained on CSIRO's F-27 research aircraft. This has been modified to take strut-mounted instruments at hardpoints at 10 locations around the fuselage 0.8 m ahead of the propeller line (see Fig. 1). Included in the standard suite of instruments are a CSIRO hot-wire probe (King *et al.*, 1978), an FSSP[1] cloud droplet spectrometer, an OAP-2D-C[1] particle imager, and an OAP-300-Y[1] precipitation particle spectrometer. The liquid water probe was mounted at either location I or E at 58.1 cm from the fuselage, and the FSSP, 2D-C and 300-Y probes at locations G, D and H respectively, all at 45 cm from the fuselage. Each strut is attached to the aircraft by bolting to a base which protrudes 70 mm from the fuselage and is 125 mm wide at its maximum width.

In addition to these instruments, a second CSIRO hot-wire probe and a small pitot-static tube were mounted on the end of a small strut that could be retracted into the aircraft during flight, thus enabling measurements of LWC and air velocity to be taken at various distances from the skin. Pressurization was maintained via plastic seals around the aerofoil strut section. Details of the hot-wire probe and pitot tube are shown in Fig. 2. This retractable strut could be located at positions E, D, C, and B. The hot-wire probe could be varied from 15 to 60 cm from the skin, with the pitot an extra 2.5 cm farther out. The pitot-static tube was a standard Prandtl design (Goldstein, 1965), and when it was calibrated against the laboratory's standard pitot-static tube in a small wind tunnel, the derived velocities were found to be within 0.5% for angles of attack up to 50°.

3. Airflow measurements

In taking the measurements described below, the air velocities derived from the retractable pitot were

[1] Manufactured by Particle Measuring Systems, Boulder, CO.

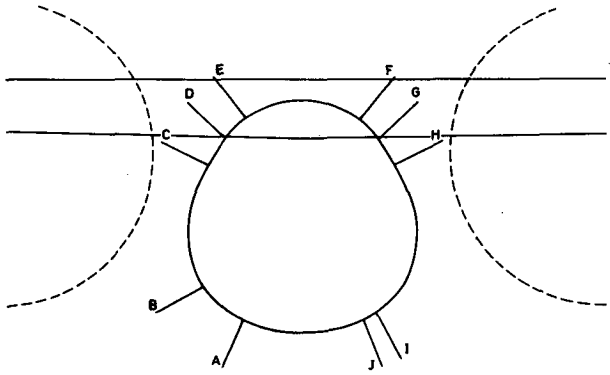

FIG. 1. View of the F-27 looking aft, showing the 10 probe locations. These are 0.8 m ahead of the propeller disk, shown dashed. The wing root region, for which the quarter-chord line is 3.8 m behind the line of the probe sites, is also shown.

normalized to those obtained from the pilot's reference air-speed indicator which samples from a pitot-static tube 30 cm forward of the wing tip. This system in turn was calibrated by precise timing over a known course (out and back) on a calm early morning flight. For a total of six runs, the pilot's system was found to read 0.99 ± 0.01 of the true aircraft velocity. The small correction necessary has been taken into account.

A typical data set for position B is shown in Fig. 3.

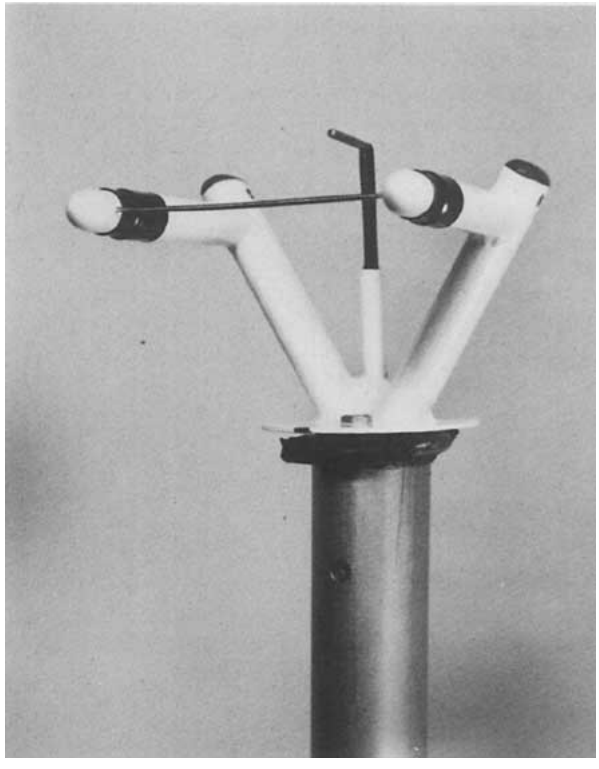

FIG. 2. Details of the retractable hot-wire probe and pitot-static tube.

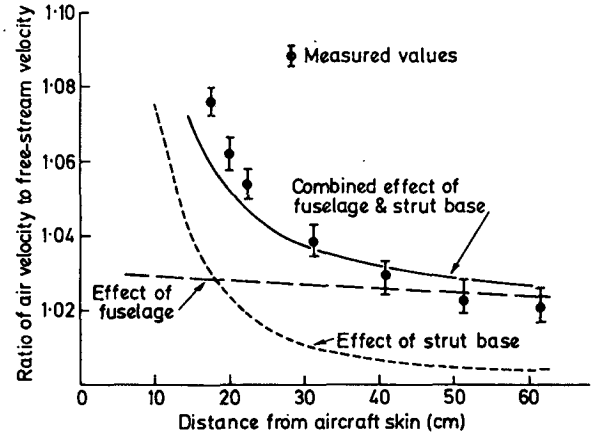

FIG. 3. Calculated increases in air velocity due to the strut base (short dash line), the fuselage (long dash line), and the combined effect of both (continuous line). These are in reasonable agreement with measurements taken at site B with the starboard engine shut down and the propeller feathered.

These results were taken on descent at 82 m s^{-1} indicated air speed with the starboard engine shut down and the propeller feathered (the effects of propeller inflow will be discussed later). Also shown in Fig. 3 are the calculated values for Q_t/V (Q_t is the local air speed, V the free-stream velocity) for (i) flow around the aircraft fuselage alone and (ii) flow around the strut base alone. Velocities for both these bodies were calculated in the manner described in Part I. An interesting feature of these calculations is that for distances from the skin less than 18 cm, the strut base has a larger effect on increasing the flow velocities than the fuselage does—a reflection of the fact that in terms of scaled distances the pitot was closer to the nose of the strut base than the nose of the aircraft.

If the overall velocity increase is regarded as being the product of these two separate effects (a reasonable approach, since the flow incident upon the strut base is fairly uniform over its depth) then the calculated increase as shown in Fig. 3 is in reasonable agreement with the measured ones, indicating the usefulness and accuracy of the sink–source technique.

4. Liquid water content measurements

That the magnitude of sampling errors can indeed be as large as those calculated in Part I is well illustrated by the data shown in Fig. 4, where we have plotted LWC from the retractable probe at 20, 25, and 60 cm from the skin at location E against values obtained from the fixed probe at location I. At 20 cm, where the retractable probe is sampling only about one-quarter the LWC of the fixed one, the close-in one is undoubtedly inside the shadow zone. From Part I we can calculate that for a shadow zone of this width, much of the LWC must be in drops whose diameters are greater than 80 μm diameter, a feature readily ob-

servable from 2-D images obtained at the same time. At 25 cm the retractable probe is sometimes in an enhancement region, reading up to 30% higher than the fixed probe, and at 60 cm it is sampling within 5% of the fixed probe, with both sampling close to free-stream conditions. Thus the ratio of one probe output to another can vary by a factor of 5 for a distance change of only 45 cm.

Although the data shown in Fig. 4 is quite useful in a qualitative sense for illustrating the magnitude of the sampling problem, it is somewhat difficult to analyse on a quantitative basis. For many reasons (not the least of which is uncertainty in the sampling cross-section of particles which appear as images of the 25–125 μm size range of the 2-D probe) it has been found that a quantitative analysis is only possible on those data sets for which a reasonable fraction of the total LWC is contributed by particles sampled by the FSSP probe, i.e., 3–45 μm diameter.

On this basis we have attempted to correct data similar to that of Fig. 4 (but of much less striking appearance because the droplets are smaller) using enhancement factors calculated in the same manner as given in Part I. Because the hot-wire probes provide a measure of the third moment of the droplet spectrum, these corrections need to be made using enhancement factors weighted according to the LWC in each size interval, i.e., the free-stream LWC w_f was obtained from the measured LWC w_m according to $w_f = w_m/e$, where

$$e = \frac{\sum_{i=1}^{15} n_i a_i^3 E(a_i)}{\sum_{i=1}^{15} n_i a_i^3}. \quad (1)$$

In (1) the symbols refer to n_i drops in each of 15 size bins from the FSSP probe. Each bin size is centered around drops of radius a_i, and $E(a_i)$ is the enhancement factor for this size drop. (Note that E also depends on aircraft speed, air viscosity, and fuselage radius in the manner described in Part I, and in this paper the enhancement factor also includes the small calculated increases in air velocity due to flow around the aircraft shape.) Only two basic sets of enhancement factors were computed—one for points above the aircraft in the vertical plane of symmetry, the other for points below the lower surface in the plane of symmetry. The top set was used for location E, and the lower set for locations I, B and C, each being modified appropriately to take account of the radius of curvature of the fuselage in the plane of interest. The lower set was used for location C because although it is closer to the top, the air moving past there does not pass over the cockpit hump and moves around a slowly changing shape more akin to the bottom surface. In any case, the maximum difference between the two enhancement factor sets at any given location was less than 3% for drops less than 50 μm in diameter. No corrections were applied to the FSSP dataset itself, since this would effectively constitute a second-order effect.

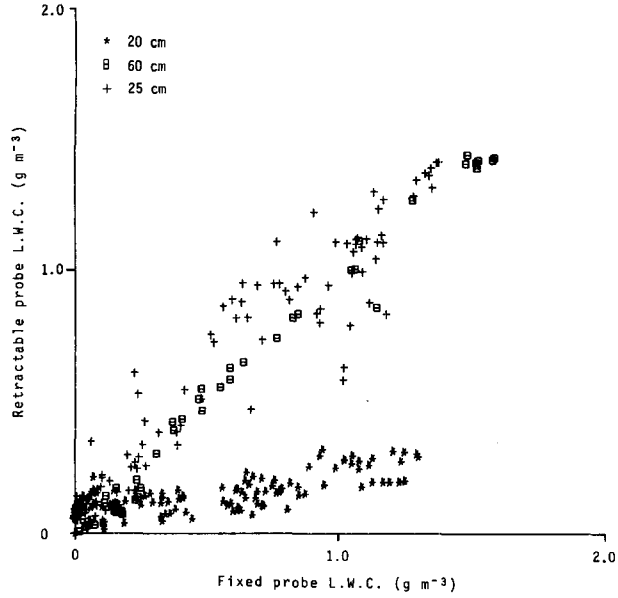

FIG. 4. Showing the wide differences in LWC that can be obtained by sampling at different distances from the skin. Data obtained at location E (retractable) and I (fixed) at about 80 m s^{-1}.

All computations are based on 1-s averages of aircraft data from small to medium cumulus clouds and marine stratocumulus, most of it obtained at 70 m s^{-1}, with some limited datasets at 110 m s^{-1}. Data from both CSIRO probes was processed in the manner described in King *et al.* (1981), except that a separate dry calibration was not performed for the retractable hot wire for every distance on every probe position. Rather, a single calibration was performed at the maximum distance at location B, and the small constant residuals caused by the different flow velocities at the different positions, amounting to no more than an equivalent of 0.05 g m^{-3}, were subtracted from each separate data set.

Examples of data corrected in this manner are shown in Figs. 5 and 6, with Fig. 5 showing the uncorrected data and Fig. 6 the corrected. Correcting for fuselage-generated enhancement factors has obviously decreased the total scatter as well as decreasing the slope of the best-fit line by about 8% to bring it very close to unity. Indeed, this dataset by itself would appear to be a good demonstration of the manner in which the enhancement factors could be used to correct for sampling errors as well as confirming the approach taken in Part I.

5. Other locations

Unfortunately, this does not represent the entire picture since we also have comparable data sets for

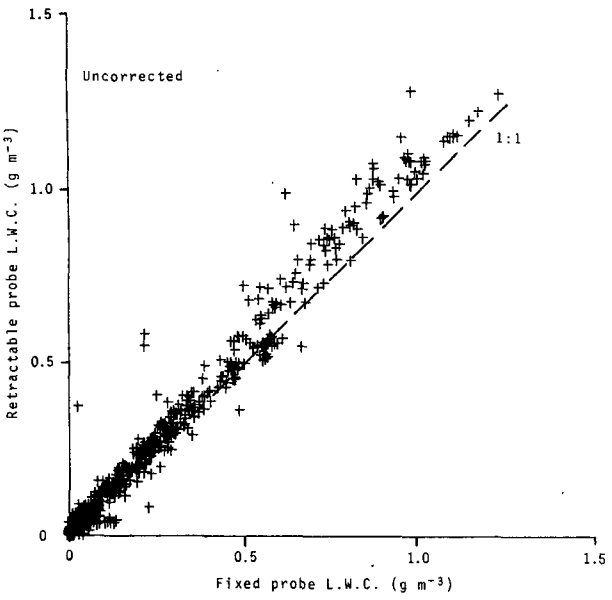

FIG. 5. Raw data collected at location E (retractable) and I (fixed). Retractable probe varied from 15 to 60 cm from the skin. Fixed probe at 58.1 cm from the skin. Mean droplet diameter = 15 μm.

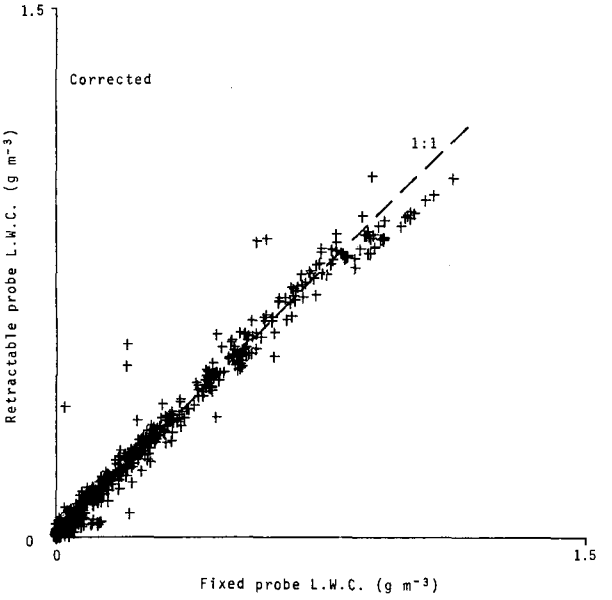

FIG. 6. Same data as in Fig. 5, but corrected for concentration enhancements. The scatter is noticeably less, and the slope of the best fit line very close to unity.

other combinations of probe positions for which the corrected 15 cm data is very close to the corrected 60 cm data (a good indication that the appropriate corrections have been made), but both are definitely different from a 1:1 relationship with the fixed probe. Table 1 lists the slopes of the best-fit lines describing the relation between retractable and fixed probes, for the other combinations of probe locations used.

Since neither of the hot-wire probes nor the method of analysis was changed from one location to another, and the departures from unity slope are statistically significant at the 1% level, the obvious inference is that there are further sampling errors, albeit less than 20%, which have not been taken into account. In fact, if we make the assumption that for each probe site there is a multiplicative sampling error, and also a multiplicative error associated with each hot-wire probe, then Table 1 can be used to establish a set of equations which can shed light on the relative magnitudes of these errors. Letting the error factor for the retractable and fixed probes be r and f respectively and the error of each site be $p_A \cdots p_I$, then the contents of Table 1 can be written as

$$p_E r = 1.08 p_I f, \quad (2)$$

$$p_B r = 1.09 p_I f, \quad (3)$$

$$p_C r = 1.18 p_I f, \quad (4)$$

$$p_B r = 0.99 p_E f. \quad (5)$$

Solution of this set of equations then leads us to the following values (where we have referred the site errors to site I, since we regard this as being the one most likely to be closest to free-stream conditions): $r/f = 0.98$, $p_B/p_I = 1.11$, $p_C/p_I = 1.20$ and $p_E/p_I = 1.10$.

It is reassuring that the ratio of probe outputs (r/f) found using this technique is close to unity, giving support to the fact that both probes respond to the same effect in the same manner (a characteristic that has not always been displayed by other liquid water measuring devices—see Strapp and Schemenauer, 1982). However, the magnitudes of the ratios of the error factors for some of the probe positions is a little disturbing, and in the following section we discuss possible causes.

6. Other possible sampling errors

a. Insufficient correction

For those probe positions for which the retractable probe sampled higher values than the fixed, the retractable probe was generally closer to the skin (in a normalized sense) even when fully extended. One possible cause of the unexplained effects noted above could be that the calculated enhancement factors were too

TABLE 1. Ratio of LWC from retractable probe to LWC from fixed probe for various site combinations and data obtained at 70–80 m s^{-1}.

		Fixed probe	
		I	E
Retractable probe	B	1.09	0.99
	C	1.18	
	E	1.08	

small: large enhancement factors for both probes would have had the effect of making the slope of the best-fit line closer to unity. Underestimates of the calculated enhancement factors could have occurred if some of the LWC sampled by the probes was contributed by drops outside the size range of the FSSP, for which we have made no corrections. Although this is known to be the case for some data sets, a partition of them according to whether the concentration of drops sampled by the 2D probe (lowest detectable size about 40 μm) was less than 5 L^{-1} produced no change in slope greater than 2%, so this does not appear to be a major factor.

There are three other reasons why it appears unlikely that the enhancement factors are grossly in error:

(i) Application to each subset of data resulted in corrected lines which were fairly constant and independent of the distance from the skin. Therefore if the calculated enhancement factors are incorrect, they have to be in error by a constant amount which is independent of distance from the skin. This is considered unlikely.

(ii) The same enhancement factor data sets were applied to all probe positions, yet the results depend only on the position—not the mean diameter nor any of the other spectrum-related features that have marked effects on the calculation of enhancement factors.

(iii) The enhancement factors were calculated in the same manner as Part I, where they were found to be in good agreement with those of Norment and Zalosh (1974).

b. *Induced velocities due to lift of the wing and fuselage*

Flow velocities over the hot-wire probes which were in excess of the free-stream velocity would have been interpreted as higher LWC. An obvious place to look for such effects would be at site E, where upwash over the wing root area could be important. An estimate of upwash velocities can be obtained by considering the induced velocities of a vortex system equivalent to a wing with lift. The simplest and most widely used of such systems considers the wing as a horseshoe vortex consisting of three vortex filaments of strength Γ—a fixed one along the wing span at the quarter-chord line and two other of semi-infinite length trailing from the wing tips (Milne-Thomson, 1966). We are here primarily interested in the induced velocity component in the direction of travel, i.e., $u' = u_{xw}\cos\alpha + u_{zw}\sin\alpha$, where α is the angle of the wing with respect to the horizontal, and u_{xw} and u_{zw} are the induced velocity components parallel and perpendicular to the wing chord respectively. For points near the centre-span these are given by (Milne-Thomson, 1966)

$$u_{xw} = \frac{\Gamma z s}{2\pi}(x^2 + z^2)(x^2 + z^2 + s^2)^{-1/2}, \quad (6)$$

$$u_{zw} = -\frac{\Gamma x s}{2\pi}(x^2 + z^2)(x^2 + z^2 + s^2)^{-1/2}, \quad (7)$$

where s is the wing semi-span (14.5 m), x the distance along the chord (upstream is negative) and z the distance above the chord. For probe position E, at the maximum extension of the pod, the coordinates are $x = 3.7$, $z = 0.36$ m. For the F-27 with a typical all-up mass of 1.5×10^4 kg and a wing area of 70 m^2, the angle of attack at an indicated air speed of 60 m s^{-1} (corresponding to a true air speed of 70 m s^{-1} at an air density of 0.9 kg m^{-3}) can be calculated as 9.8°. Since the line of zero lift is at −3° to the horizontal the effective angle of attack for our purposes is 6.8°, and using (6) and (7) we find $u' = 8.9 \times 10^{-3}\Gamma$. Now the circulation Γ is related to the lift L of a wing with elliptic loading by $\Gamma = 2L/\pi\rho_a V s$ (Glauert, 1942), where ρ_a is the density of air. Using the same values as before, we find $u' = 0.94$ m s^{-1}, or a 1.3% increase in flow velocity. This reduces to only 0.3% at 110 m s^{-1}. (The relative error u'/V varies approximately as V^{-2} because the circulation required to generate a given lift decreases as V^{-1}.)

In a similar vein, one can calculate disturbance velocities (i.e., perturbations on the free-stream velocity) around the fuselage associated with the lift generated by it at small angles of attack. These velocities are most easily described in circular cylindrical polar coordinates x, r, θ with the cylindrical axis along the center of the fuselage (x positive in the direction of flow), the polar angle θ measured from the center top of the fuselage, and r the cylindrical radial coordinate. With this system, the disturbance velocities are given by (Munk, 1963)

$$u_{xf} = V\sin\beta\cos\theta\frac{\partial S}{\partial x}(\pi r)^{-1}, \quad (8)$$

$$u_{rf} = V\sin\beta\cos\theta\left(1 - \frac{S}{\pi r^2}\right), \quad (9)$$

$$u_{\theta f} = -V\sin\beta\cos\theta\left(1 + \frac{S}{\pi r^2}\right), \quad (10)$$

where S is the area of a section at right angles to the x axis and β is the angle of the flow relative to the fuselage. In this case we shall take $\beta = \alpha - \epsilon$, where α is the effective angle of attack of the wing as already used and ϵ is the fixed angle between the wing and the fuselage (3.5° at the wing root for the F-27). In fact, at certain places around the fuselage β could be as much as 50% greater than $\alpha - \epsilon$ owing to upwash over the wings, but we shall ignore these complications in this simple treatment. In any case, it should be noted that the effective angle of attack of the fuselage can vary from 3.3° to −3.3° in going from 60 to 90 m s^{-1} indicated air speed.

At the top and bottom of the aircraft ($\cos\theta = 1, -1$ respectively) we find at the position of the probes,

where $\partial S/\partial x \approx 0.6$ m, that $u_{xf}\cos\beta/V'$ is ~0.8% on the top and −0.8% on the bottom for a combined difference of 1.6%. At 90 m s^{-1} however the signs are reversed.

At the sides of the aircraft the axial and radial components vanish, and although the polar component is equal to twice the cross-flow velocity here (i.e., $2V\sin\beta$), its component along the horizontal is still negligibly small.

The net result of these calculations on the disturbance velocities associated with the lift of the wings and fuselage is that when combined, they can account for no more than about one-third of the 10% difference in LWC sampled at 70 m s^{-1} at sites E and I. Nevertheless, similar LWC measurements at higher speeds support the premise that much of these differences is in fact related to angle-of-attack effects (see Figs. 7 and 8). Both data sets are displays of data corrected on the basis of fuselage enhancement factors only, and include data for the retractable probe at positions from 15 to 60 cm from the skin. Fig. 7 shows data gathered at about 70 m s^{-1}, while that in Fig. 8 was gathered at 110 m s^{-1}. It is apparent that increasing the aircraft speed has removed almost all of the remaining unexplained sampling differences between sites E and I. For those situations in which the sampling instrument is not particularly sensitive to sampling speed, it may well be better to sample at higher speeds to eliminate the lift-associated disturbance velocities and correct for the fuselage distortion enhancement factors in the manner of Part I.

c. *Inflow into the propellers*

While the induced velocities discussed in Section 6b can help explain the sampling errors associated with upper and lower probe positions, the same reasoning cannot be applied to locations B and C, which are more off to the side of the aircraft. An inspection of Table 1 and Fig. 1 shows that location C, which has the largest sampling error, is also the one closest to the propeller disk, and this fact prompted the following analysis of what the inflow velocities into the propeller region might be.

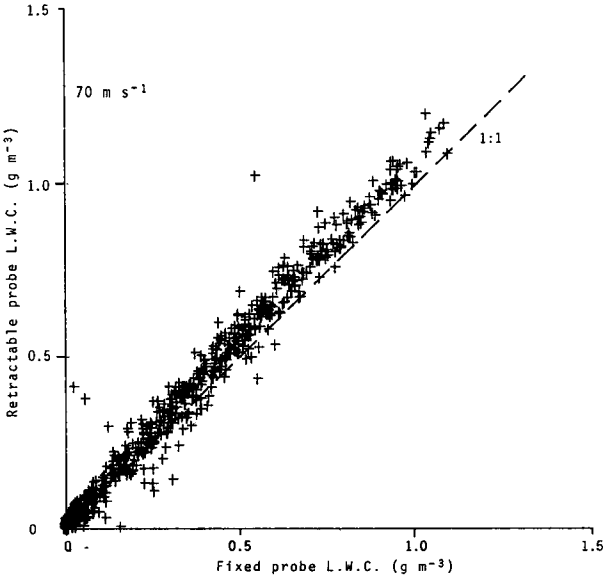

FIG. 7. Data obtained at 70 m s^{-1} at locations E (retractable) and I (fixed). Corrected for concentration enhancements.

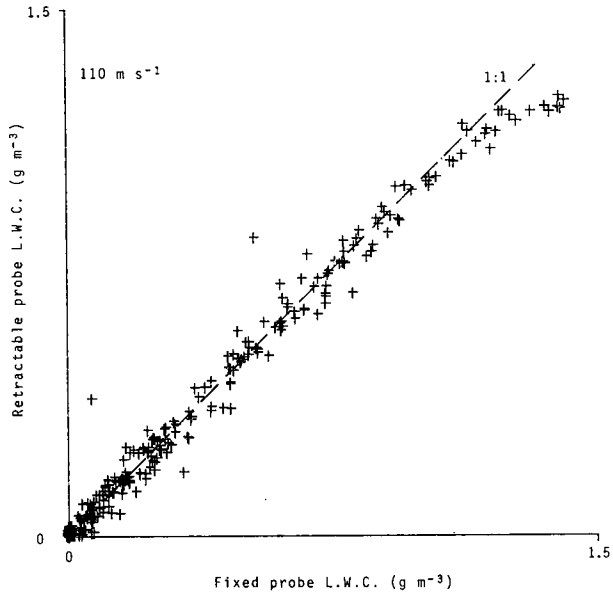

FIG. 8. Data similar to that in Fig. 7, but collected at 110 m s^{-1}. Note that the slope is much closer to unity.

The simplest propeller theory assumes that the propeller is an isolated solid disk across which there is a pressure discontinuity, that the velocity downstream is increased by an amount v, and that this increase is related to the propeller thrust T via a momentum balance equation given by

$$v(V+v) = \frac{T}{2\pi R^2 \rho_a}, \tag{11}$$

where R is the propeller radius (Milne-Thomson, 1966).

Now the maximum continuous power available from an F-27 engine is 1.15×10^6 W at sea level. Allowing for a degradation of this power with density differences at altitude and for a propeller efficiency of 0.8, we arrive at a figure of a maximum of 7.5×10^5 W of propeller power available at an altitude of 2.0 km under conditions of a standard ICAN atmosphere. This in turn implies a thrust of 1.25×10^4 N at 60 m s^{-1} and 8.33×10^3 N at 90 m s^{-1}. Solving (11) gives values for v of 8.59 m s^{-1} at $V = 60$ m s^{-1} and 4.19 m s^{-1} at $V = 90$ m s^{-1}.

For our purposes we are interested in the inflow region upstream of the propeller, and with the theory given by Koning (1963) the radius (r_s) of this region at a distance x upstream of the propeller disk, can be calculated as

$$r_s = R\left\{1 + \frac{v/Vx}{2(R^2 + x^2)^{1/2}}\right\}. \quad (12)$$

Inside this region the axial velocity disturbance is given

$$u'_{xp} = v[1 - x(R^2 + x^2)^{-1/2}]. \quad (13)$$

At the position of the pod mounts, $x/R = 0.44$, so we find that $u'_{xp} = 5.13$ m s^{-1} and 2.5 m s^{-1} and $r_s/R = 1.029$ and 1.009 for $V = 60$ and 90 m s^{-1} respectively. The important features are, therefore, that the disturbance velocities can be quite large inside the propeller inflow region, but that this inflow region is only slightly larger than the propeller diameter. An inspection of Fig. 1 shows that, except at the position of maximum extension for position C, it is unlikely that any hot-wire probe was inside the direct inflow.

Outside the inflow zone, the axial and radial velocities are equivalent to those flowing into a sink of magnitude $2\pi R^2 v$ at the propeller center. Thus,

$$u'_{xp} = -\frac{1}{2} vR^2 x(x^2 + r^2)^{-3/2}, \quad r > r_s, \quad (14)$$

$$u'_{rp} = -\frac{1}{2} vR^2 r(x^2 + r^2)^{-3/2}, \quad r > r_s. \quad (15)$$

Because of the proximity of the fuselage, these expressions for an isolated propeller are not strictly correct, but some simple calculations using image techniques show that the real axial component should not be more than 30% above that given in (14). Substitution of appropriate values for x, r and R shows that u'_{xp}/V will be of the order of 3% for $V = 60$ m s^{-1} and 1% at 90 m s^{-1}.

These calculations can be compared with measurements of flow velocities at location B under conditions

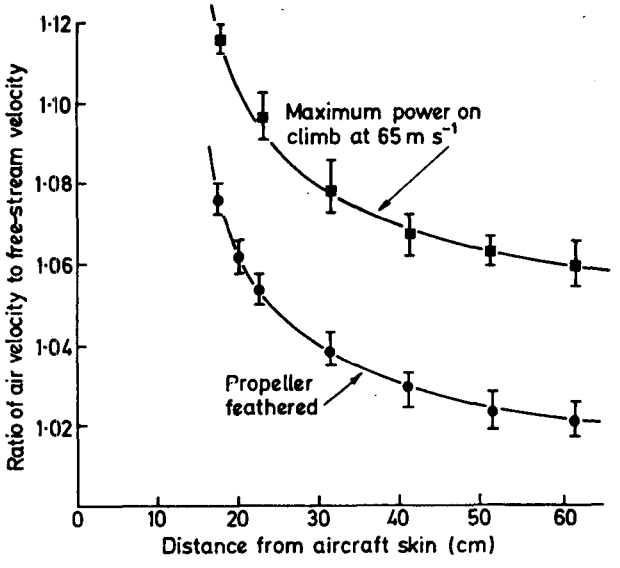

FIG. 9. Effects of propeller on air velocity at location B. Operation of the starboard engine at maximum continuous power has increased velocities by about 4%.

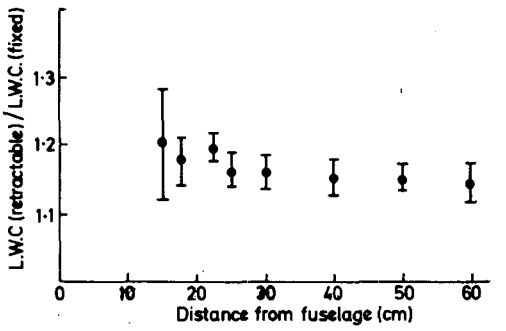

FIG. 10. Ratio of retractable to fixed LWC as a function of distance from the skin for the retractable probe at C and the fixed probe at I.

in which the starboard engine was used at maximum continuous power. The true air speed was 62 m s^{-1} and the temperature and pressure were close to those for the International Standard Atmosphere for an average altitude of 2 km. Fig. 9 shows that increases in u'_{xp}/V over and above the values for when the starboard engine was shut down are of the order of 4%, slightly more than was calculated for flows outside the propeller inflow region. Thus for site B there is reasonable agreement between the airflow measurements and the theory.

A comparable dataset for site C at 90 m s^{-1} in level flight with both engines operative showed increases in velocity due to propeller effects of the order of 3%. The magnitude as calculated using the techniques above is only 0.75%, so the measured effect at C is about four times larger than expected. In terms of LWC, not only are the sampling errors as shown in Table 1 for sites B and C much larger than the measured airflow increases, but they also both show very little dependence on distance from the skin (see Fig. 10); so it seems unlikely that either was in the direct inflow region. It is possible that changes in the direction of flow caused by the propellers (rather than a direct velocity increase) could be responsible for concentration enhancements in the same manner as the fuselage distorts the flow and causes similar effects. Any investigation of these effects would be quite complex. Further investigations would also have to include those effects due to the turbulent nature of air flow around an aircraft, i.e., studies of how fluctuating angles of attack, roll and sideslip could influence measurements of both particle concentrations and turbulent particle fluxes.

7. Discussion

From the foregoing, it is obvious that the fuselage is not the ideal location for many direct sampling instruments, a fact well recognized by researchers over the years and currently evident in the increasing use of wing-mounted instruments. Nevertheless, wing mounting will not eliminate sampling problems altogether, and in any case, there are often situations in

which fuselage mounting is very desirable, if not necessary (e.g., for use with retractable direct sampling devices). When employing fuselage-mounted instruments the user needs to be aware of the types and magnitudes of sampling errors that can be encountered. In this paper we have dealt with three types of sampling errors due to flow distortions around the fuselage, wings and propellers. Conclusions which could be made on the basis of this work include the following:

- Sampling errors due to fuselage shape effects can be as large as 400% for drops of the order of 100 μm diameter, in line with the theory of Norment and Zalosh (1974) and King (1984). Even when the mean droplet diameter is only 20 μm sampling errors can be as large as 20%, but the work described here suggests they can be corrected to an accuracy of a few percent. The magnitude of the fuselage shape effects increases with sampling speed.
- Sampling errors associated with flows over lifting bodies such as the wings and perhaps to a lesser extent the fuselage, are more difficult to deal with. However, the indications from the F-27 work suggest that they are unlikely to be more than 10% at 60 m s^{-1} and that they decrease as the inverse square of the aircraft velocity.
- The sampling errors due to propeller inflows could be quite large for units mounted directly ahead of or behind the propellers (perhaps as large as 14% in the F-27 situation). Away from the sites nearest the propellers the effects are again likely to be less than 10% at 60 m s^{-1}, decreasing approximately as the inverse square of aircraft velocity.
- The comparative precision of the CSIRO liquid water probe is probably of the order of a few percent, but the probes would need to be mounted much closer together than was done in this study to test this accurately. The best comparison results of the two probes were obtained when flying at the higher speeds, using the enhancement factors calculated in the manner of Part I to correct for the fuselage distortion effects, and relying on the fact that the other effects of propellers, wings and fuselage all decrease with increasing speed. In this way, apparent differences of the order of 20% were decreased ~3%. For some situations this may well be the best approach to adopt.

During the course of this study it became obvious very early that probe/probe comparisons were not easy, even when both were mounted on the same aircraft. The difficulties involved in two-probe comparisons in which the probes were on different aircraft would be considerably greater, and the sum total of the types of errors described here would need to be considered for both aircraft before any inferences about the relative performance of the probes themselves could be drawn.

Acknowledgments. The authors are grateful to Laurel Arthur for computing assistance, to S. C. Mossop and M. MacInante for help with the PMS probes, and to C. E. Coulman and M. A. Parker for the use of a second CSIRO probe.

REFERENCES

Glauert, H., 1942: *Elements of Aerofoil and Airscrew Theory.* Cambridge University Press, 232 pp.

Goldstein, S., 1965: *Modern Developments in Fluid Dynamics.* Dover, 702 pp.

King, W. D., 1984: Air flow and particulate trajectories around aircraft fuselages. Part I: Theory., *J. Atmos. Ocean. Technol.*, **1**, 5–13.

——, D. A. Parkin and R. J. Handsworth, 1978: A hot-wire liquid water device having fully calculable response characteristics. *J. Appl. Meteor.*, **17**, 1809–1813.

——, C. T. Maher and G. A. Hepburn, 1981: Further performance tests on the CSIRO liquid water probe. *J. Appl. Meteor.*, **20**, 195–202.

Koning, C., 1963: In *Aerodynamic Theory: A General Review of Progress.* W. Durand, Ed., Vol. IV. Dover.

Milne-Thomson, L. M., 1966: *Theoretical Aerodynamics.* MacMillan, 430 pp.

Munk, M., 1963: *Aerodynamic Theory: A General Review of Progress,* Vols. I, VI. W. Durand, Ed. Dover.

Norment, H. G., and R. G. Zalosh, 1974: Effects of airplane flow fields on hydrometeor concentration measurements. Rep. No. AFCRL-TR-74-0602, Air Force Cambridge Research Lab, 101 pp.

Strapp, W. J., and R. S. Schemenauer, 1982: Calibrations of Johnson-Williams liquid water content meters in a high-speed icing tunnel. *J. Appl. Meteor.*, **21**, 98–108.